Chaotic chirped-pulse oscillators

Evgeni Sorokin,[1,*] **Nikolai Tolstik,**[2] **Vladimir L. Kalashnikov,**[1] **and Irina T. Sorokina**[2]

[1]*Institut für Photonik, TU Wien, Gusshausstrasse 27/387, A-1040 Vienna, Austria*
[2]*Department of Physics, Norwegian University of Science and Technology, N-7491 Trondheim, Norway*

[*]*sorokin@tuwien.ac.at*

Abstract: We present results of experimental investigation of the chaotic and quasi-periodic regime in the chirped-pulsed (dissipative soliton) Cr:ZnS and Cr:ZnSe mid-IR oscillators with significant third-order dispersion. The instability develops when the spectrum edge approaches resonance with a linear wave either due to power increase or by dispersion adjustment. In practice, this occurs when the spectrum edge reaches zero dispersion wavelength. The analysis suggests a three-oscillator chaos model, which is confirmed by numerical simulations. The regime is long-term stable and can be easily overlooked in similar systems. We show that chaotic regime is accompanied by a characteristic spectral shape and can be reliably recognized by using wavelength-skewed filters and by second-harmonic or two-photon absorption detectors.

OCIS codes: (140.3580) Lasers, solid-state; (140.7090) Ultrafast lasers; (140.4050) Mode-locked lasers; (140.1540) Chaos; (190.3100) Instabilities and chaos.

References and links

1. W. H. Renninger, A. Chong, and F. W. Wise, "Area theorem and energy quantization for dissipative optical solitons," J. Opt. Soc. Am. B **27**, 1978–1982 (2010).
2. V. L. Kalashnikov, E. Podivilov, A. Chernykh, and A. Apolonski, "Chirped-pulse oscillators: theory and experiment," Appl. Phys. B **83**, 503–510 (2006).
3. T. M. Kardas, W. Gadomski, B. Ratajska-Gadomska, and P. Wasylczyk, "Automodulations in an extended cavity, passively modelocked Ti:Sapphire oscillator - period doubling and chaos," Opt. Express **18**, 26989–26994 (2010).
4. E. Sorokin, V. L. Kalashnikov, J. Mandon, G. Guelachvili, N. Picque, and I. T. Sorokina, "Cr^{4+}:YAG chirped-pulse oscillator," New J. Phys. **10**, 083022 (2008).
5. S. Kobtsev, S. Kukarin, S. Smirnov, S. Turitsyn, and A. Latkin, "Generation of double-scale femto/pico-secondoptical lumps in mode-locked fiber lasers," Opt. Express **17**, 20707–20713 (2009).
6. L. Wang, X. Liu, Y. Gong, D. Mao, and L. Duan, "Observations of four types of pulses in a fiber laser with large net-normal dispersion," Opt. Express **19**, 7616–7624 (2011).
7. P. Junsong, Z. Li, G. Zhaochang, L. Jinmei, L. Shouyu, S. Xuehao, and S. Qishun, "Modulation instability in dissipative soliton fiber lasers and its application on cavity net dispersion measurement," J. Lightwave Technol. **30**, 2707–2712 (2012).
8. S. Smirnov, S. Kobtsev, S. Kukarin, and A. Ivanenko, "Three key regimes of single pulse generation per round trip of all-normal-dispersion fiber lasers mode-locked with nonlinear polarization rotation," Opt. Express **20**, 27447–27453 (2012).
9. Q. Wang, T. Chen, M. Li, B. Zhang, Y. Lu, and K. P. Chen, "All-fiber ultrafast thulium-doped fiber ring laser with dissipative soliton and noise-like output in normal dispersion by single-wall carbon nanotubes," Appl. Phys. Lett. **103**, 011103 (2013).
10. N. Tolstik, E. Sorokin, and I. T. Sorokina, "Kerr-lens mode-locked Cr:ZnS laser," Opt. Lett. **38**, 299–301 (2013).
11. E. Sorokin and I. T. Sorokina, "Ultrashort-pulsed Kerr-lens modelocked Cr:ZnSe laser," in *European Conference on Lasers and Electro-Optics and the European Quantum Electronics Conference - CLEO Europe - EQEC*, (IEEE, München, 2009), p. CF1_3.

#197666 - $15.00 USD Received 13 Sep 2013; revised 10 Nov 2013; accepted 14 Nov 2013; published 22 Nov 2013

12. E. Sorokin, N. Tolstik, and I. T. Sorokina, "1 Watt femtosecond mid-IR Cr:ZnS laser," Proc. SPIE **8599**, 859916 (2013).
13. V. L. Kalashnikov, E. Sorokin, and I. T. Sorokina, "Chirped dissipative soliton absorption spectroscopy," Opt. Express **19**, 17480–17492 (2011).
14. N. N. Akhmediev and A. Ankiewicz, *Solitons: Nonlinear Pulses and Beams* (Chapman and Hall, 1997), Vol. 4.
15. E. Podivilov and V. L. Kalashnikov, "Heavily-chirped solitary pulses in the normal dispersion region: new solutions of the cubic-quintic complex Ginzburg-Landau equation," JETP Lett. **82**, 467–471 (2005).
16. V. L. Kalashnikov, A. Fernández, and A. Apolonski, "High-order dispersion in chirped-pulse oscillators," Opt. Express **16**, 4206–4216 (2008).
17. H. R. Telle, G. Steinmeyer, A. E. Dunlop, J. Stenger, D. H. Sutter, and U. Keller, "Carrier-envelope offset phase control: A novel concept for absolute optical frequency measurement and ultrashort pulse generation," Appl. Phys. B **69**, 327–332 (1999).
18. G. P. Agrawal, *Nonlinear Fiber Optics*, 4th ed. (Academic, 2006).
19. V. L. Kalashnikov, "Dissipative solitons: perturbations and chaos formation," in *Chaos Theory. Modeling, Simulation and Applications*, C. H. Skiadas, I. Dimotikalis, and C. Skiadas, eds. (World Scientific, 2011), pp. 199–206.
20. N. Tolstik, I. T. Sorokina, and E. Sorokin, "Watt-level Kerr-lens mode-locked Cr:ZnS laser at 2.4 μm," in *CLEO: Science and Innovations* (Optical Society of America, San Jose, 2013), p. CTh1H.2.
21. C. Spielmann, P. F. Curley, T. Brabec, and F. Krausz, "Ultrabroadband femtosecond lasers," IEEE J. Quantum Electron. **30**, 1100–1114 (1994).
22. N. Tolstik, I. T. Sorokina, A. Pospischil, and E. Sorokin, "Graphene mode-locked Cr:ZnS laser with 44 fs pulse duration," in *Advanced Solid-State Lasers Congress*, M. Ebrahim-Zadeh and I. Sorokina, eds. (Optical Society of America, Paris, 2013), p. MW1C.1.
23. V. L. Kalashnikov and E. Sorokin, "Soliton absorption spectroscopy," Phys. Rev. A **81**, 033840 (2010).
24. V. L. Kalashnikov, I. G. Poloyko, V. P. Mikhailov, and D. von der Linde, "Regular, quasi-periodic, and chaotic behavior in continuous-wave solid-state Kerr-lens mode-locked lasers," J. Opt. Soc. Am. B **14**, 2691–2695 (1997).
25. Q. Xing, L. Chai, W. Zhang, and C.-Y. Wang, "Regular, period-doubling, quasi-periodic, and chaotic behavior in a self-mode-locked Ti:sapphire laser," Opt. Commun. **162**, 71–74 (1999).
26. J.-H. Lin and W.-F. Hsieh, "Three-frequency chaotic instability in soft-aperture Kerr-lens mode-locked laser around 1/3-degenerate cavity configuration," Opt. Commun. **225**, 393–402 (2003).
27. J. M. Soto-Crespo, M. Grapinet, P. Grelu, and N. Akhmediev, "Bifurcations and multiple-period soliton pulsations in a passively mode-locked fiber laser," Phys. Rev. E **70**, 066612 (2004).
28. F. Li, P. K. A. Wai, and J. N. Kutz, "Geometrical description of the onset of multi-pulsing in mode-locked laser cavities," J. Opt. Soc. Am. B **27**, 2068–2077 (2010).
29. H. I. Choi and W. J. Williams, "Improved time-frequency representation of multicomponent signals using exponential kernels," IEEE Trans. Acoust. Speech Signal Process. **37**, 862–871 (1989).
30. B. Per, B. Tomas, and J. Mogens Høgh, "Mode-locking and the transition to chaos in dissipative systems," Phys. Scr. **1985**, 50–58 (1985).
31. V. L. Kalashnikov and A. Chernykh, "Spectral anomalies and stability of chirped-pulse oscillators," Phys. Rev. A **75**, 033820 (2007).
32. C. Baesens, J. Guckenheimer, S. Kim, and R. S. MacKay, "Three coupled oscillators: mode-locking, global bifurcations and toroidal chaos," Physica D Nonlinear Phenomena **49**, 387–475 (1991).
33. D. Pazó, E. Sánchez, and M. A. Matías, "Transition to high-dimensional chaos through quasiperiodic motion," Int. J. Bifurc. Chaos **11**, 2683–2688 (2001).
34. H. D. I. Abarbanel, R. Brown, J. J. Sidorowich, and L. S. Tsimring, "The analysis of observed chaotic data in physical systems," Rev. Mod. Phys. **65**, 1331–1392 (1993).
35. L. A. Aguirre, "A nonlinear correlation function for selecting the delay time in dynamical reconstructions," Phys. Lett. A **203**, 88–94 (1995).
36. M. B. Kennel, R. Brown, and H. D. I. Abarbanel, "Determining embedding dimension for phase-space reconstruction using a geometrical construction," Phys. Rev. A **45**, 3403–3411 (1992).

1. Introduction

Mode-locked oscillators operating in the all-normal $(\beta_2 > 0)$ dispersion regime (ANDi) have established themselves as versatile sources of energy scalable chirped picosecond pulses, which can be further compressed to well below hundred femtosecond duration. The main interest in implementing such sources is the possibility to generate high-energy pulses directly from an oscillator, avoiding complex and costly amplifier schemes. These chirped-pulse oscillators (CPO) operate in the dissipative soliton (DS) regime, which is somewhat more complex than a soliton-like compensation of self-phase modulation by anomalous dispersion as in conventional femtosecond lasers. A minimum set of parameters that are required for the CPO regime to exist

#197666 - $15.00 USD Received 13 Sep 2013; revised 10 Nov 2013; accepted 14 Nov 2013; published 22 Nov 2013

includes additionally a spectral bandwidth filter and a saturable (e.g. nonlinear-optical) absorber [1, 2]. On top of that, the higher-order dispersion is often unavoidable in broadband systems. As a result, the CPOs are described by a quite complicated multidimensional parameter space; on practice one can often encounter increased amplitude or spectral noise, period multiplication and modulational instability, noise-like and chaotic behaviour [3–9]. It is important therefore to establish the physical mechanisms, properties, and find practical rules to help recognising such regimes.

In this paper, we describe and characterize the observed chaotic regimes in the chirped-pulse Cr:ZnS and Cr:ZnSe lasers [10, 11] and confirm our physical model with the numerical simulations. We demonstrate that the chaotic mode-locking in a solid-state oscillator results from a parametric resonance with dispersive waves, having different signature and mechanism than observed in the fiber lasers [5–9].

2. Experimental setup and observations

The chaotic regime of a Cr:ZnSe mode-locked laser has been reported for the first time in 2009 [11]. The Kerr-Lens mode-locked (KLM) CPO with a bulk dispersion compensation by a YAG plate exhibited significant third-order dispersion (TOD) originated from the active medium itself, the bulk compensator, and the cavity mirrors.

More detailed experiment on the chaotic behavior was carried out recently with a KLM Cr:ZnS laser (Fig. 1). The laser was pumped by a 5W polarized Er-fiber laser emitting at 1.61 μm. The astigmatically-compensated delta-cavity was characterized by 146 MHz repetition rate and 1.7% outcoupling rate. The Brewster-mounted diffusion-doped Cr:ZnS crystal was passively cooled by a copper heatsink. The laser was operated at average output powers of 35–70 mW resulting in the output pulse energies of 0.25–0.5 nJ (15–30 nJ intracavity energy), though much higher output power could be achieved in this cavity both in femtosecond regime [10] and in CPO regime [12]. A pair of Brewster-oriented YAG wedges provided continuous tuning of the second-order dispersion (GDD) with the constant TOD at +8200 fs^3. Substituting the mirror M1 by a chirped mirror with subsequent compensation by the thickness of YAG wedges resulted in negligible TOD [Fig. 1(c)] and forced the laser to operate in the regular chirped pulsed regime. The pulse duration varied between 1.7–2.0 ps at spectrum widths of 110–140 cm^{-1}, giving the time-bandwidth product of 6.5–8.5.

The detecting of chaotic and quasiperiodic regimes of a mode-locked laser is an issue. The output pulse energy does not fluctuate in these regimes: the power noise on a fast photodiode is at the same level, as with a regular chirped-pulse or femtosecond soliton regime. The laser spectra recorded by a slow spectrometer (for example, FTIR device) are very stable and reproducible, so monitoring of the laser spectrum and energy stability could not help in identifying the chaotic behavior. Nevertheless, the spectral instability is indeed present, but occurs at the frequencies in a hundreds-of-kilohertz range. It could however be detected by a fast photodetector with a skewed spectral filter [Fig. 1(b)] installed in front of it [Out1 in Fig. 1(a)], providing a signal related to the instantaneous central wavelength of the pulse, or by a detector operating in a two-photon absorption mode, thus sensitive to the pulse peak intensity. [The pulse spectrum $S(\lambda)$ gets multiplied by a filter transmission curve $T(\lambda)$ and collected by a detector with spectral sensitivity $V(\lambda)$. The signal at detector $V = \int S(\lambda) \cdot T(\lambda) V(\lambda)\, d\lambda$ thus becomes spectrally weighted. If the weighting function were linear $V(\lambda)T(\lambda) = a + b\lambda$ then the signal (divided by the full pulse energy measured at Out2) becomes exactly proportional to the pulse central wavelength $\lambda_0 = \int \lambda S(\lambda) d\lambda / \int S(\lambda) d\lambda$ with some baseline. While for our broadband spectra the filter transmission curve [Fig. 1(b)] cannot be considered really linear, it nevertheless allows retrieving the signal approximately equal to the central wavelength fluctuations up to the pulse repetition frequency. The numerical simulation described in Sections 3 and 4 used the actual

#197666 - $15.00 USD Received 13 Sep 2013; revised 10 Nov 2013; accepted 14 Nov 2013; published 22 Nov 2013

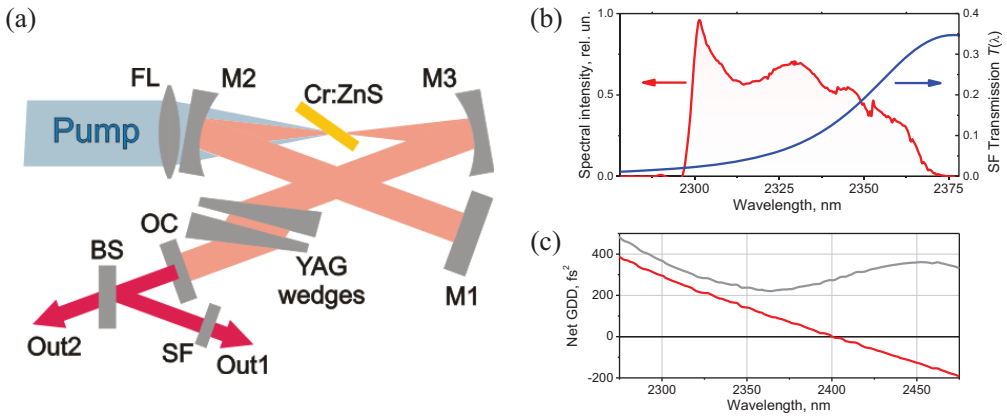

Fig. 1. (a) Schematic of the femtosecond Kerr-lens mode-locked Cr:ZnS laser: FL – focusing lens, M1, M2, and M3 – high reflector mirrors (M1 could be substituted by a chirped mirror), Cr:ZnS – active element, YAG wedges – dispersion compensation, OC – output coupler, BS – beam splitter, SF – spectral filter, Out1 –laser output for controlling the wavelength, Out2 - main laser output; (b) typical laser spectrum (red) and spectral filter transmission (blue); (c) laser cavity round-trip GDD with bulk dispersion compensation (red), and with chirped mirror dispersion compensation (grey).

transmission curve $T(\lambda)$ of the Fig. 1(b) to model the Out1 signal.] Particularly, the strong noise in the pulse interferometric autocorrelation trace arises because of the short-term pulse waveform fluctuation.

In our experiments the laser spectra were recorded by a Perkin-Elmer FTIR spectrometer with 11 kHz detector bandwidth. Even the weak narrow-band features resulting from the intracavity water vapor absorption [13] could be reliably resolved. The short-term fluctuation of the laser central wavelength was controlled by the 15-MHz extended-InGaAs photodiode with a spectral filter installed in front of it. The typical (averaged) laser spectrum and the transmission of the spectral filter are presented in Fig. 1(b). Clear modulation of the laser central wavelength with the frequencies well over 100 KHz was observed [Fig. 2(b)].

The interferometric autocorrelation traces of the laser pulses were recorded by a home-made two-photon absorption-based autocorrelator. The typical autocorrelation traces in regular and chaotic chirped regimes are plotted in Fig. 2(c), the characteristic noise can easily be recognized. The modulation of the second harmonic signal recorded by the autocorrelator's photodetector is plotted in Fig. 2(b). The modulation of the central wavelength and the modulation of the second harmonic signal are not generally correlated with each other in time, but could correlate in case of a quasiperiodic regime.

Having control on the detection of the chaotic regime, we were able to investigate the conditions of its appearance. Switching from the regular chirped to chaotic and quasi-periodic regimes was achieved by either increasing the intracavity pulse power or decreasing (positive) by translating the wedges [Fig. 3(b)]. Increasing the power at constant dispersion [horizontal line in Fig. 3(b)] results first in a small quasiperiodic modulation with a characteristic jigsaw wavelength signal (dark red dots), followed by a true chaotic regime (red dots) and then again by a quasiperiodic regime (violet dots) with wavelength and peak power signals phase-shifted by about 90 degrees.

#197666 - $15.00 USD Received 13 Sep 2013; revised 10 Nov 2013; accepted 14 Nov 2013; published 22 Nov 2013

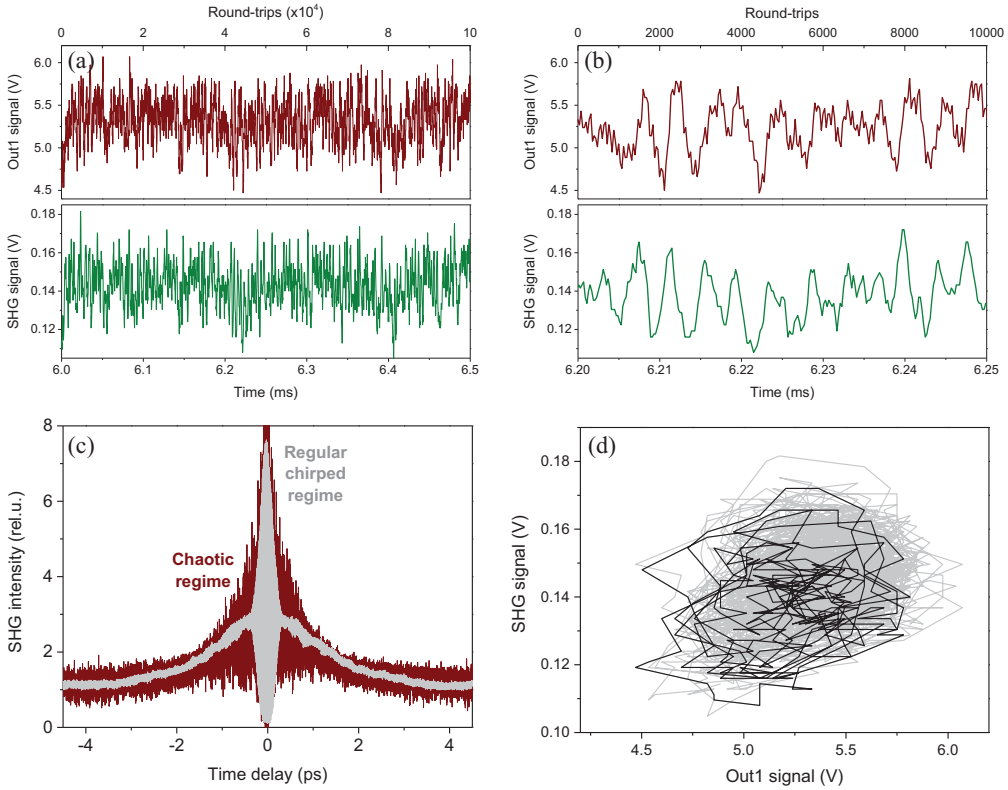

Fig. 2. Chaotic regime in time domain. (a), (b) Signals from the Out1 channel (dark red, related to the central wavelength) and second-harmonic intensity (green, related to pulse peak power) of the Cr:ZnSe CPO laser in chaotic regime. (c) Interferometric autocorrelation traces recorded with the fast detector in chaotic (dark red) and regular chirped (grey) regimes. (d) Parametric diagram corresponding to the signals on graph (a) and (b) (grey and black lines, respectively), showing uncorrelated truly chaotic behaviour.

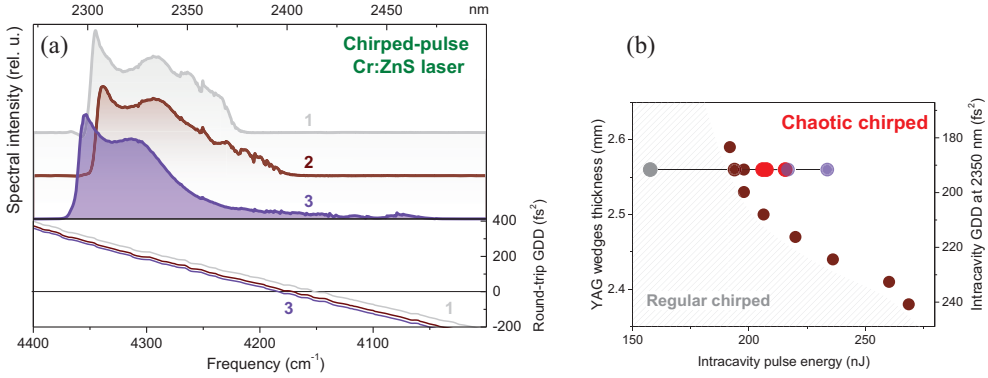

Fig. 3. Output spectra (a) and corresponding dispersion values (b) of a CPO Cr:ZnS laser in various regimes: regular CPO (spectrum 1 and grey dot); stability border between regular and chaotic (spectrum 2 and dark red dots), and chaotic (spectrum 3 and red/violet dots). The red dots denote purely chaotic regime, violet dots denote quasiperiodic regime.

#197666 - $15.00 USD Received 13 Sep 2013; revised 10 Nov 2013; accepted 14 Nov 2013; published 22 Nov 2013

3. Theoretical description and numerical modeling

In this section, we shall present a qualitative analytical model of a CPO and compare it with a soliton laser operating in the anomalous dispersion regime. We shall study the impact of the TOD using the numerical model.

3.1. Analytical description

The ultrashort pulse dynamics of mode-locked lasers can be described using the generalized complex nonlinear cubic-quintic Ginzburg-Landau equation (CNGLE) [14]. In the framework of this model, evolution of the slowly varying field amplitude $A(z,t)$ along the propagation coordinate z (cavity round-trip number in our case) can be described with the usual normalizations [15] as

$$\begin{aligned}\frac{\partial A(z,t)}{\partial z} = &\left\{-\sigma+\alpha\frac{\partial^2}{\partial t^2}+\left[\kappa\left(1-\zeta|A(z,t)|^2\right)|A(z,t)|^2\right]\right\}A(z,t)\\ &+\mathrm{i}\left\{\frac{\beta_2}{2}\frac{\partial^2}{\partial t^2}-\gamma|A(z,t)|^2\right\}A(z,t)+\frac{\beta_3}{6}\frac{\partial^3}{\partial t^3}A(z,t),\end{aligned} \tag{1}$$

where t is a local time. Dissipative factors in this system are defined by the saturated net-loss coefficient σ, squared inverse gain bandwidth α, nonlinear gain coefficient κ, and nonlinear gain saturation ζ. The latter two parameters approximate the self-amplitude modulation (SAM) of the Kerr-lens mode-locking. Nondissipative factors are defined by the group-delay dispersion (GDD) and the self-phase modulation (SPM) with the coefficients β_2 and γ, respectively. The last term in Eq. (1) accounts for the TOD [16]. Eq. (1) describes both, chirped-pulse ($\beta_2>0$) and conventional soliton ($\beta_2<0$) lasers. In the latter case, setting α, κ, and ζ to zero produces the well-known nonlinear Schrödinger equation, but for a stable chirped-pulse operation frequency filtering and SAM are required [1].

A steady-state solution of Eq. (1) should have a form $A(t,z)=E(t)\exp(-iqz)$, where the soliton wave q is related to the carrier-envelope offset [17] as $q \bmod 2\pi = \phi_{CEO} = 2\pi\nu_{CEO}/f_{rep}$. The theory based on adiabatic approximation [2,15] predicts, that a chirped dissipative soliton (CDS) of Eq. (1) with $\beta_2>0$ and $\beta_3=0$ has a wave number $q=\gamma P_0$, where P_0 is the pulse peak power (for the Schrödinger soliton $q=\gamma P_0/2$ [18]). Since $\beta_2>0$ for the CDS, there exist resonances with linear waves having the wave numbers $k(\omega)=\beta_2\omega^2/2$: $k(\pm\Delta)=q$ as opposed to the Schrödinger soliton in the anomalous ($\beta_2<0$) GDD regime (Fig. 4). Under this condition, the CDS can be stable only if its spectrum is truncated at the frequencies $\pm\Delta$, which define the CDS spectrum width. For such CDS we obtain $q=\gamma P_0=(\beta_2/2)\Delta^2$, which is the analog of the Schrödinger soliton area theorem $\gamma P_0=|\beta_2|/T_0^2$. The resonance condition implies that the position of the spectrum edges can be controlled by changing the dispersion and/or the pulse energy [(Fig. 4(a)].

The TOD contribution ($\beta_3\neq 0$ in Eq. (1)) modifies the resonant condition: $q=\beta_2\omega^2/2+\beta_3\omega^3/6$. As a result, an additional resonant frequency may appear. As was conjectured in [16, 19] approaching of third resonant frequency to the CDS spectrum is the source of chaotic dynamics. The concept of parametric resonance defined by these resonant frequencies will be the keystone for further consideration.

3.2. Numerical model

The numerical simulation of Eq. (1) followed the procedure described in [2], with the crystal divided in 10 split-step slices, 2^{18} grid points and 2.5 fs time resolution. The parameters used in simulations are $\alpha=16$ fs^2, $\kappa=0.04\gamma$, $\zeta=0.2\gamma$, and $\gamma=10$ MW^{-1}, selected to match the

#197666 - $15.00 USD Received 13 Sep 2013; revised 10 Nov 2013; accepted 14 Nov 2013; published 22 Nov 2013

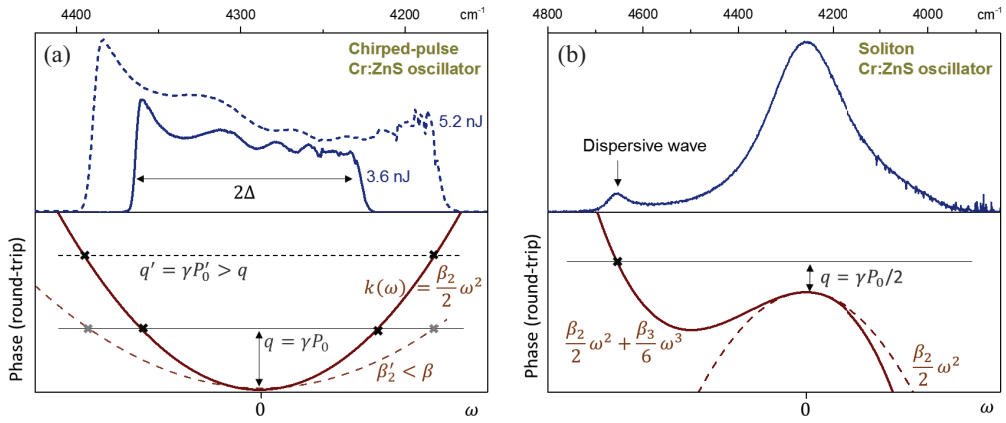

Fig. 4. (a) Resonance condition (black crosses) for the CDS defines the spectrum width 2Δ. Changing the power and/or the dispersion (dashed lines) controls the spectrum width. Blue lines show the experimental spectra [20] corresponding to different energies. (b) For the conventional soliton laser ($\beta_2 < 0$) a resonance is only possible with TOD, which generates a dispersive wave [21], illustrated by an experiment [22].The high-frequency modulation on the spectrum envelope in both graphs results from the intracavity water vapour [13, 23].

experimental conditions as close as possible. The gain saturation in the framework of Eq. (1) was taken into account by the means of near-threshold expansion [2]: $\sigma = \delta(E/E^* - 1)$, where $E = \int |A(z,t')|^2 dt'$ is the intracavity pulse energy, E^* is the energy stored in a cavity in the CW regime (it is a control parameter), and $\delta = 0.03$.

With the positive GDD, the model generated regular chirped pulses with nearly rectangular spectra. By adding the TOD, we were able to numerically reproduce the chaotic regime, as well as power and spectral dependence of the transition between regular and chaotic lasing. In the chaotic regime, the pulse spectral shape, central wavelength, time-bandwidth product, pulse duration, and chirp parameter do fluctuate without significant correlation on the time scale of 10–10^3 round-trips, while the pulse energy remains stable within 1%. This corresponds very closely to the experimental observations, except the spectrum shape. However, averaging by 7000 round-trips (this value corresponds to the actual 11 kHz detector bandwidth of the FTIR spectrometer) produced stable spectral shapes very similar to experimental spectra shown in Fig. 3. The transition to the chaotic regime could be triggered either by pulse energy increase and/or dispersion shift, like it was observed in the experiment. We are thus confident that the present numerical model adequately describes the main source of the chaotic destabilization. At the same time, the model showed broader parameter regions of true chaotic regime and almost no quasiperiodic regions like in Fig. 3. We attribute this to the approximations taken in the model: neglecting the higher-order dispersions, distributed dispersion and nonlinearity, etc. Assuming a different sign of the TOD does not change the picture, except that the spectrum and pulse waveform get mirrored, corresponding to time reversal.

4. Results and discussion

Mode-locked oscillators are known to demonstrate a variety of the dynamical scenarios including chaotic [5, 24-27]. As was demonstrated, the nonlinear gain and loss can result *per se* in a chaotic pulse dynamics [28]. In our work, a source of chaotic behavior is interpreted as a CDS resonance with dispersive waves excited by TOD.

#197666 - $15.00 USD Received 13 Sep 2013; revised 10 Nov 2013; accepted 14 Nov 2013; published 22 Nov 2013

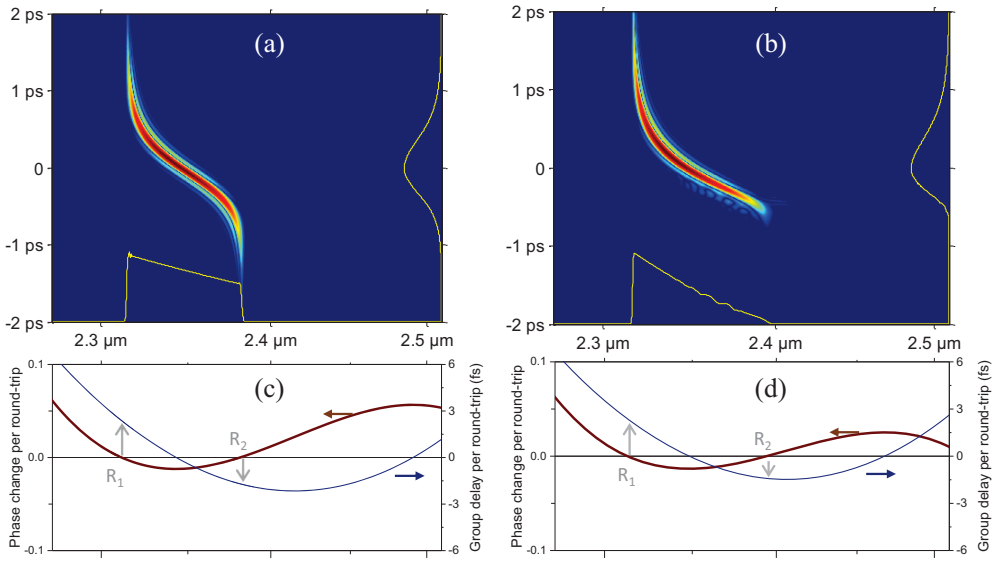

Fig. 5. Time-frequency diagrams of the regular CDS regime with small TOD (a) and large TOD (b). Pseudocolor diagrams show the amplitude of the smoothed Wigner distribution [29] in logarithmic scale. The yellow curves at the bottom and to the right show the spectrum and time intensity, respectively. (c),(d): The corresponding round-trip phase delay (dark red) and group delay (blue) curves for the linear waves. Gray arrows denote the edge tails generated at the resonance positions R_1 and R_2.

To understand the impact of the TOD, it is instructive to consider the time-frequency diagrams of the CDS (Fig. 5). At relatively low TOD [Fig. 5(a)] the pulse corresponds to that of the approximate model of Fig. 4: it consists of a linearly chirped central part and the two tails at spectrum edges, which are very well localized in frequency at resonance positions R_1 and R_2. The addition of the TOD only results in trapezoidal spectrum shape [Fig. 5(a) and spectrum 1 in Fig. 3] and slight asymmetry of the tails. Higher amount of TOD changes the spectrum shape to near triangular [Fig. 5(b) and spectrum 2 in Fig. 3], corresponding to collapse of the long-wavelength tail. More importantly, the dispersive wave resonance [third zero-crossing of the phase delay curve in Fig. 5(d)] is now approaching the spectrum. Further TOD increase brings the dispersive wave resonance (DW) position sufficiently close to the pulse [Fig. 6(c)], so that the corresponding dispersive wave gets excited. Since DW position corresponds the positive group delay, the dispersive wave would propagate slightly faster than the pulse, with about a fraction of optical period (≈8 fs) per round-trip. Practically, it overlaps in time with both, the tail corresponding to the R_2 edge and the main part of the CDS. The interference and nonlinear interaction of three waves results in complete change of the whole spectrum and chaotic behavior (Fig. 6). The spectrum and waveform of the pulse [Fig. 6(a), yellow lines] acquire strong modulation, which is rapidly changing (see Media 1). Yet the average spectrum, accumulated over 7000 round-trips (corresponds to the detector time constant of 20 kHz) is stable and reproduces the characteristic “boa constrictor digesting an elephant” asymmetric shape with a long tail at one side ending with a small peak [spectrum 3 in Figs. 3 and 6(d)]. The experimentally accessible GDD curve crosses zero at a point where group delay reaches

#197666 - $15.00 USD Received 13 Sep 2013; revised 10 Nov 2013; accepted 14 Nov 2013; published 22 Nov 2013

its minimum. Comparing Figs. 5(c), 5(d), and 6(c), we can note that transition to chaos also *approximately* coincides with zero GDD position reaching the edge of the spectrum; this can serve as a convenient practical rule in experimental work.

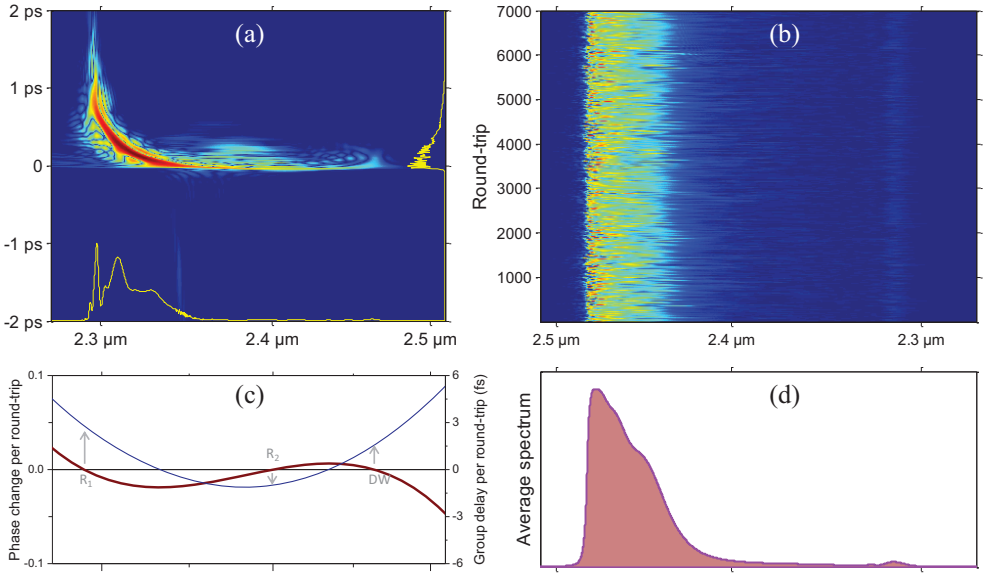

Fig. 6. Chaotic CDS regime. (a) Time-frequency diagram of a typical single round-trip and a corresponding round-trip phase and group delays (c). Spectra (b) of the 7000 round-trips and their accumulated spectrum (d), corresponding to the actual detector time constant. Media 1 provides the animated sequence of (a) and accumulation of (d) over the 7000 round-trips, as well as time dependencies of the pulse energy, SHG, wavelength, and r.m.s. spectral width.

We thus conclude that our model adequately describes the experiment and that the TOD is indeed responsible for the onset of the chaotic instability: as the resonant wavelength approaches the pulse spectrum, the corresponding dispersive wave merges with the pulse edge and becomes strongly amplified. This merger can be a result of either dispersion change, as illustrated in Fig. 3, or pulse power increase with associated spectrum broadening. Both mechanisms have been observed in the experiment and in the simulation. Since the dispersive wave now overlaps with the pulse both spectrally and in time, their interference results in modulation, both in spectral and time domain. Normally, this would result just in modulation, but strong nonlinear interaction in the active medium causes the chaotic regime. As was shown above, the CDS is coupled with the dispersive waves that defining the soliton spectrum truncation. Under these conditions, CDS can exhibit a chaotic behavior even in the presence of only two resonant frequencies [30]. Such behavior was interpreted as an excitation of the internal CDS perturbation modes [31]. Contribution of a third resonant frequency $(\beta_3 \neq 0)$ enhances the tendency to chaotic behavior, which can be described as a nonlinear resonance of three coupled oscillators [32,33].

This is not the only possible mechanism for chaotic destabilization of the CPOs. In a number of recent works, fiber lasers operating in net-normal dispersion regimes have demonstrated noise-like and multi-state behavior [5,6,8,9], that was attributed to saturation of the SAM. These systems operated well in the positive dispersion with relatively small TOD, and produced completely different signatures, such as nearly symmetric spectra and bell-shaped autocorrelation traces with a narrow coherence spike at the top, thus allowing clear distinguishing from the

#197666 - $15.00 USD Received 13 Sep 2013; revised 10 Nov 2013; accepted 14 Nov 2013; published 22 Nov 2013

TOD-related chaotic state as discussed here.

To characterize the chaotic regime, we reconstruct the phase-space portrait for the experimental CDS dynamics based on the standard lag-delayed procedure [Fig. 7(a)]. The lag-value defined by the first zero of the peak power set correlation function [34] was 2.44 μs ($\sim$350 round-trips), but as was pointed in [35] the most representative lag-value is smaller due to contribution of nonlinear effects.

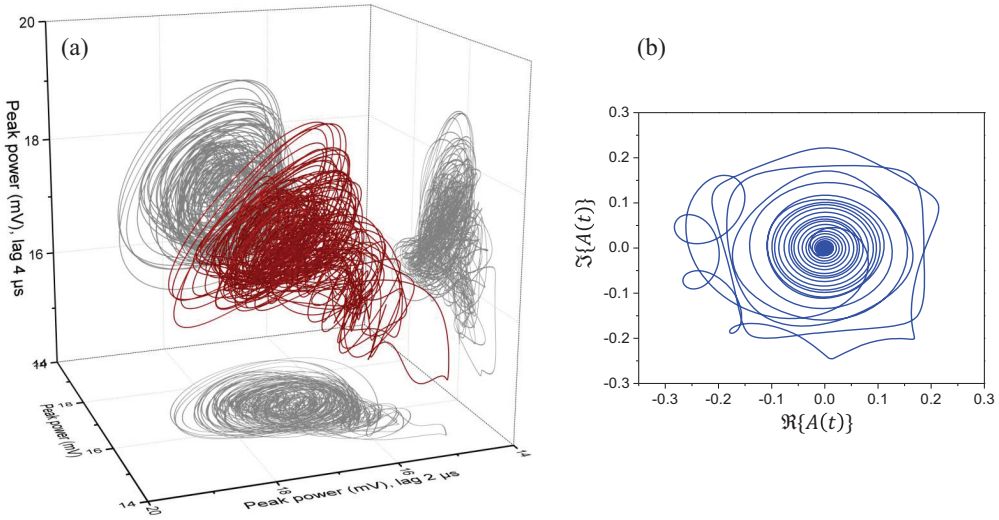

Fig. 7. (a) Phase portrait of the experimental CDS peak power set for 210 nJ of intracavity pulse energy. The 2 μs lag corresponds to 290 round-trips. The high-frequency detector noise is removed by the Fourier-filtering. (b) Calculated instantaneous phase portrait of a CDS. The wandering trajectory demonstrates the phase distortion and changes irregularly between the round-trips. The regular helicoidal trajectory corresponds to the pulse tail at the short-wavelength edge.

The analysis of phase-space embedding dimension was based on the "false neighbors" method [34, 35, 36]. The representative dimensions of embedding phase-space d_{emb} in both experiment and numerical simulations were found to be $2 < d_{emb} < 4$. Fig. 7(a) demonstrates a typical toroidal shape of the attracting manifold in the phase-space. Both facts are coherent with the concept of chaos induced by the nonlinearly entangled three oscillators. Since the third resonant frequency caused by TOD affects nearest truncating frequency defining the CDS spectral shape, the CDS behaves quasi-periodically or chaotically as a whole. This behavior is clearly visible on the CDS phase portrait in Fig. 7(b), where the distortion of phase trajectory displays a chaotic wandering of the CDS instant phase at the intrapulse femtosecond time scale.

5. Conclusion

In summary, using the example of chirped-pulse mode-locked Cr:ZnS and Cr:ZnS lasers we have observed and established the nature of chaotic behaviour in solid-state CPOs, which occur when the dispersive wave merges with the pulse. This occurs when the frequency, which provides a resonant interaction between the pulse and the dispersive wave, approaches the pulse spectrum edge due to dispersion decrease and/or power increase. In practice, it is more convenient to watch out for the spectrum edge reaching the zero GDD wavelength, which is an experimentally accessible parameter. The analysis based on the chaos theory demonstrates a typical phase-space dimension around 3 and an attracting manifold of toroidal type. These facts

#197666 - $15.00 USD Received 13 Sep 2013; revised 10 Nov 2013; accepted 14 Nov 2013; published 22 Nov 2013

confirm that the chaotization of CPO dynamics can be interpreted in the framework of three nonlinear coupled oscillators model, where two resonant frequencies define the CDS spectral width and the third frequency corresponds to the dispersive wave excited by the TOD.

In the chaotic and quasiperiodic regimes, spectral and temporal shapes rapidly fluctuate on the scale of 10–1000 roundtrips, but are stable at time scales above 10000 roundtrips. The fluctuations can be observed using fast detectors, but may remain unnoticed when standard spectral devices are used. A typical signature of the chaotic regime is the characteristic shape of the spectrum edge with a long tail ending with a peak. From a practical point of view, the chaotic regime is stable on the long-term time scale and has smooth predictable spectrum, making possible its use in such applications as high-resolution molecular spectroscopy.

Acknowledgments

This work was supported by the Austrian Science Fund (FWF): project P24916-N27, and the Norwegian Research Council (NFR): projects FRITEK/191614, MARTEC-MLR, Nano 2021 N219686.

#197666 - $15.00 USD Received 13 Sep 2013; revised 10 Nov 2013; accepted 14 Nov 2013; published 22 Nov 2013